



Study on Semi-Solid A380 Aluminum Alloy Slurry Prepared by Water-Cooling Serpentine Channel and Its Rheo-Diecasting

Zhiyong Liu^{1,2} · Weimin Mao² · Tan Wan³ · Guotao Cui¹ · Weipan Wang²

Received: 9 January 2020 / Accepted: 24 February 2020 / Published online: 17 March 2020
© The Korean Institute of Metals and Materials 2020

Abstract

The semi-solid A380 aluminum alloy slurry prepared by water-cooling serpentine channel and its rheo-diecasting were studied in this paper. The result showed that the pouring temperature and cooling water flow rate had a significant effect on the semi-solid slurry. When the pouring temperature decreased from 670 to 610 °C, the average grain diameter and shape factor of the primary α -Al grains decreased from 64 to 47 μm and increased from 0.74 to 0.82, respectively, but the mass of semi-solid slurry blocked in channel increased. With the cooling water flow rate increasing from 0 to 1000 L/h, the semi-solid slurry firstly got optimized and then deteriorated. Under the condition of the same die casting process parameters, the rheo-diecastings produced by the semi-solid slurry prepared through water-cooled serpentine channel had higher mechanical properties than those of the traditional die castings.

Keywords Water-cooling serpentine channel · Semi-solid A380 aluminum alloy slurry · Rheo-diecasting · Mechanical properties

1 Introduction

Compared with the traditional die casting, the rheo-diecasting adopts the semi-solid slurry with the smooth filling and few solidified shrinkage, which makes the solidification defects reduce obviously, resulting in the rheo-diecastings having excellent mechanical properties [1, 2]. Moreover, the mechanical properties of rheo-diecastings can be further improved by heat treatment [3, 4]. Most of all, the rheo-diecasting has the advantages of high efficiency and low cost, compared with the porosity free die casting, such as vacuum die casting [5, 6] and pore-free die casting [7, 8]. The rheo-diecasting process is widely applied to the production field of the high performance or thin-wall die castings [9]. However, the rheo-diecasting depends on the semi-solid slurry that is decided by preparation process [10, 11].

The preparation of the semi-solid slurry mainly includes two mainstream theories that are controlling grain growth and improving effective nucleation ratio. In the early stage of the development of the semi-solid slurry, Flemings [12] got the semi-solid slurry by mechanical stirring which could make the grains grow in the form of non-dendrites. Zhang [13] used rotating electromagnetic field to shear the melt, which improved the temperature field and concentration field of solid–liquid interface to inhabit dendrite growth. In addition, the formation of a great many nucleation cores within quite short time in melt can inhabit dendrite growth. Lu [14] cooled the melt to the near liquidus temperature, which makes a large number of effective nucleation cores form in melt during pouring, in this way, the semi-solid slurry with near spherical or spherical grains can be obtained. At present, researchers have developed many preparation processes of the semi-solid slurry combining the two mainstream theories [15–18]. FAN [19] designed a double screw device to shear the melt at high speed, the nucleation cores formed on the inner wall, and the shearing could take the nucleation cores into melt and improve solid–liquid interface. Hirata [20] used the chilling nucleation and shearing effect of the vibrating plate to prepare the semi-solid slurry. Mahathaninwong [21] injected inert gas into the melt to form bubbles

✉ Zhiyong Liu
yyaffe@126.com

¹ School of Mechanical and Electrical Engineering, Heze University, Heze 274015, Shandong, China

² School of Materials Science and Engineering, University of Science and Technology Beijing, Beijing 100083, China

³ School of Materials Science and Engineering, University of Tsinghua Beijing, Beijing 100084, China

that could enhance heat dissipation and disturb the melt, thus obtaining semi-solid slurry.

We propose a water-cooled serpentine channel pouring process, the chilling effect of channel and "self stirring" of melt make the preparation of semi-solid slurry simple, low cost and suitable for rheological forming of the short process. In this paper, the effects of pouring temperature and cooling water flow rate on the semi-solid slurry were studied, and the rheo-diecasting was studied through comparing the macrostructures, microstructures, mechanical properties and fracture morphologies of the rheo-diecastings and traditional die castings.

2 Experiments

2.1 Materials

Commercial A380 aluminum alloy was used, whose chemical compositions (wt%) consist of Si 7.83, Cu 3.2, Fe ≤ 0.21 , Mg ≤ 0.02 , Mn ≤ 0.46 (balance Al). The solidus and liquidus temperatures of A380 aluminum alloy were 525 °C and 596

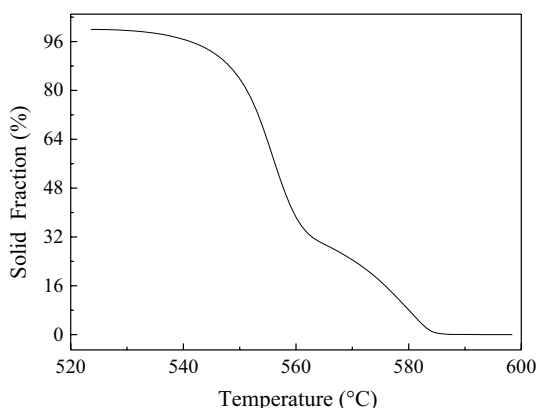


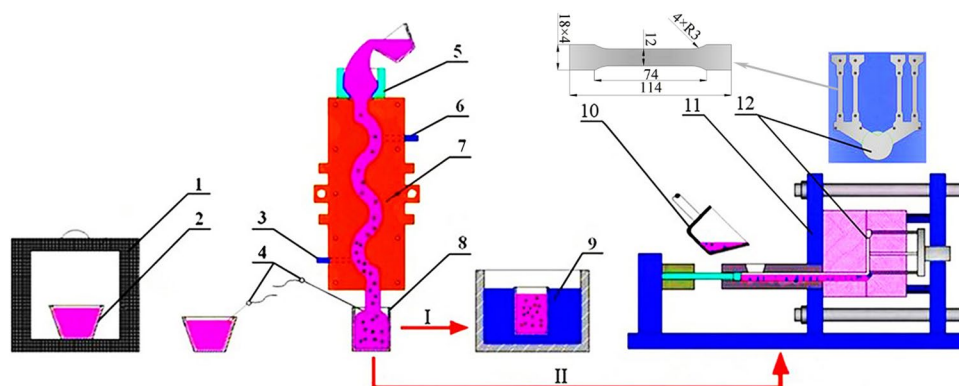
Fig. 1 Curve of solid fraction versus temperature

°C, respectively, as shown in Fig. 1, which was tested by differential scanning calorimetric method. During the test, the A380 aluminum alloy was melted at the heat rate of 10 °C/min.

2.2 Methods

The A380 aluminum alloy with 3.5 kg was melted in a graphite clay crucible ($\Phi 155 \times h 185$ mm) by the resistance furnace. The alloy melt was cooled to 700 °C and poured into the water-cooling serpentine channel that had four bends whose diameter was 30 mm. The water-cooling serpentine channel was assembled by two symmetrical cooper blocks that had half serpentine groove and cooling water seal cavity. The surface of inner wall was coated by TiN and TiCN, it could be used repeatedly by opening and assembling the two symmetrical cooper blocks. Moreover, the cooling water in the water-cooling serpentine channel came from an open system whose temperature was about 20 °C. The melt in the water-cooling serpentine channel became the semi-solid slurry under the chilling effect of the inner wall and the self-stirring of the melt and flew out the channel. On the one hand, the semi-solid slurry was collected by stainless steel crucible and quenched in water rapidly to analyze the microstructure of the semi-solid slurry, the process parameters were shown in Table 1. On the other hand, the semi-solid A380 aluminum alloy slurry was immediately transferred into the shot sleeve using a preheated preservation ladle to study the rheo-diecasting, as shown "I" in Fig. 2. In addition, the traditional die casting was carried out. The mold of standard tensile samples was used, on set of mold can produce four tensile samples once a time, as shown "II" in Fig. 2. The tensile samples of the rheo-diecasting and traditional die casting had the same pouring temperature and die casting parameter, the mold was preheated to about 200 °C, the injection pressure was 70 MPa, the slow shot speed was 0.5 m/s, and the fast shot speed was 2 m/s.

Fig. 2 Schematics of the semi-solid slurry preparation and its rheo-diecasting. 1. Resistance furnace; 2. graphite clay melting crucible; 3. cooling water inlet; 4. thermocouple; 6. tooling water outlet; 5. pouring cup; 7. serpentine channel; 8. collecting crucible; 9. cooling water; 10. Heat preservation ladle; 11. horizontal die casting machine; 12. mold cavity



I: Preparation of semi-solid A380 slurry; II: Rheo-diecasting of semi-solid A380 Aluminum alloy slurry

Table 1 The preparation and characteristic parameters of semi-solid slurry

Sample no.	Pouring temperature (°C)	Water flow rate (L h ⁻¹)	Collected slurry (g)	Blocked slurry (g)	Grain diameter (μm)	Shape factor
A	610	500	1594	492	47	0.82
B	630	500	1617	345	50	0.81
C	650	500	1582	267	56	0.78
D	670	500	1608	214	64	0.74
E	630	0	1633	281	53	0.79
F	630	1000	1612	533	57	0.72

The center of the water quenched semi-solid slurry and the middle of the tensile samples were made into the standard metallographic specimens whose microstructures were observed using a Neuphoto21 optical microscope. The Image-Pro Plus analysis software was used to analyze the average grain diameter and shape factor of the primary α -Al grains, which were calculated by $D = \sum_{i=1}^N \sqrt{4A/\pi}/N$ and $F = N / \sum_{i=1}^N [C^2/(4A\pi)]$, respectively [22]. Where D , F , A , N , and C are the average diameter, shape factor, area, number, and perimeter of the primary α -Al grains, respectively. In addition, the macrostructure of the tensile samples were observed by SG3100 low-powered optical microscope.

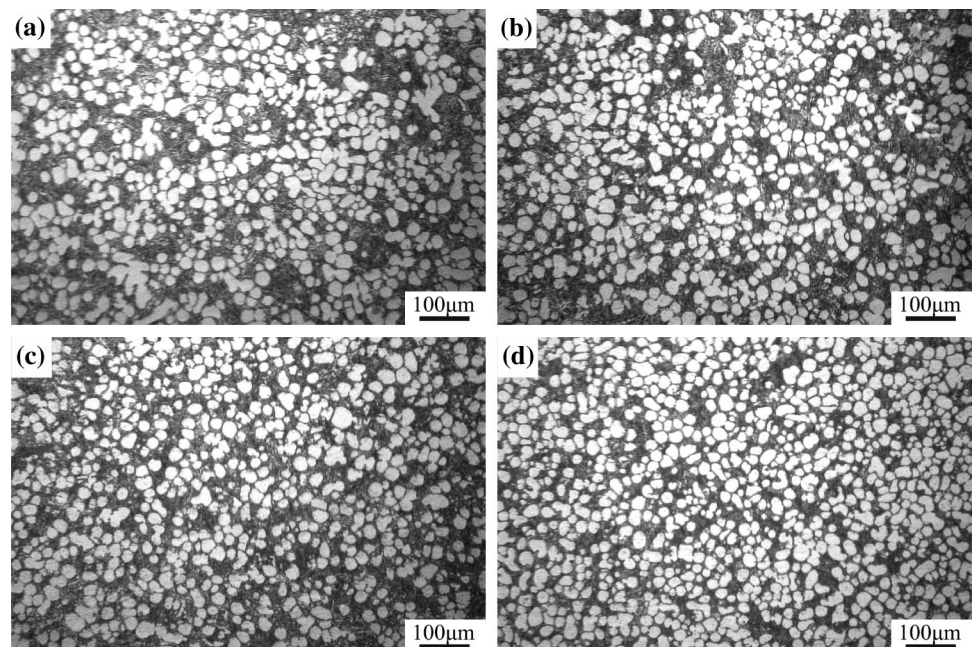
The stress-strain curve of the tensile samples were obtained by CMT4105 universal tensile test machine according to the GB/T 228.1-2010, the strain rate was 1 mm/min. Three tensile samples with same process parameters were randomly selected for mechanical properties test to ensure the reliability. The fracture morphology, fracture surface composition and microstructure nearby the fracture were observed using a ZEISS SUPRA40 scanning electron microscope, energy dispersive X-ray spectroscopy, and a

Neuphoto21 optical microscope, respectively. The Vickers hardness of the tensile samples was measured by HVS-10 hardness tester, and each test point was tested for three times, the loading and holding time were 98.07N and six seconds, respectively.

3 Results

3.1 Effect of pouring temperature on semi-solid slurry

Figure 3 was the microstructures of the semi-solid slurry, which were prepared by water-cooling serpentine channel with 500 L/h water flow rate under different pouring temperatures. The white particles were primary α -Al grains, the dark region among the primary α -Al grains was quenched solidification structure formed by residual melt. When the pouring temperature was 670 °C, there were a lot of degenerated dendrites and fractured dendritic arms in semi-solid slurry except for a few rose-like or granular grains, resulting

Fig. 3 Microstructure of semi-solid slurry prepared by different pouring temperature. **a** 670 °C; **b** 650; **c** 630 °C; **d** 610 °C

in the size difference between the primary α -Al grains obviously, as shown in Fig. 3a. The grain diameter and shape factor of the primary α -Al grain were 64 μm and 0.74, respectively. Even so, it was got optimized significantly compared with the semi-solid slurry prepared by graphite serpentine channel [22]. With the pouring temperature decreased to 650 $^{\circ}\text{C}$, the number of the dendrites and dendritic arms decreased significantly, at the same time, the number of the rose-like and near spherical grains increased, which made the uniformity of primary α -Al grain get improvement, as shown in Fig. 3b. The grain diameter reduced to 56 μm and the shape factor improved to 0.78. When the pouring temperature dropped to 630 $^{\circ}\text{C}$, the dendrites and dendritic arms almost disappeared, the primary α -Al grains were mainly spherical or near spherical, therefore, the size difference between the primary α -Al grains was very small, as shown in Fig. 3c. The grain diameter and shape factor were 50 μm and 0.81, respectively. With the pouring temperature decreased from 630 to 610 $^{\circ}\text{C}$, the morphology and grain size of the primary α -Al grain varied slightly, as shown in Fig. 3d. The grain diameter and shape factor only decreased 3 μm and increased 0.01, respectively. From Fig. 3, it is not hard to find that the distance between the primary α -Al grains gradually decreased with the pouring temperature decreasing. Figure 4a showed that the grain diameter and

shape factor obviously decreased and increased, respectively when the pouring temperature decreased from 670 to 630 $^{\circ}\text{C}$. When the pouring temperature dropped from 630 to 610 $^{\circ}\text{C}$ they changed slightly. However, the variation trends of the blocked slurry ratio (blocked slurry divided by collected slurry) was opposite to above changing trends, especially when the pouring temperature decreased from 630 to 610 $^{\circ}\text{C}$, the blocked slurry ratio increased sharply, as shown in Fig. 4b. The optimum pouring temperature was 630 $^{\circ}\text{C}$, under the situation of comprehensively considering the quality and availability ratio of the semi-solid slurry.

3.2 Effect of Water Flow Rate on Semi-solid Slurry

Figure 5a, b were the microstructures of semi-solid slurry prepared by water-cooling serpentine channel with 0 L/h and 1000 L/h water flow rate, respectively, whose pouring temperature was 630 $^{\circ}\text{C}$. When the water flow rate was 0 L/h, the primary α -Al grains of the semi-solid slurry were mainly composed of the rose-like and granular grains, and the rose-like grains accounted for a large proportion. The grain diameter and shape factor were 53 μm and 0.79, respectively. When the water flow rate increased to 1000 L/h, there were quite a considerable number of degenerated dendrites, fracture dendritic arms in semi-solid slurry, resulting in the grain

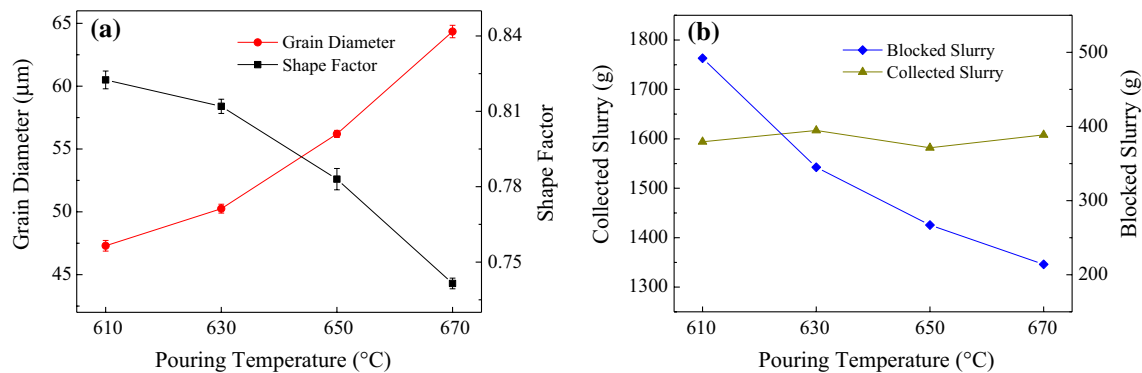
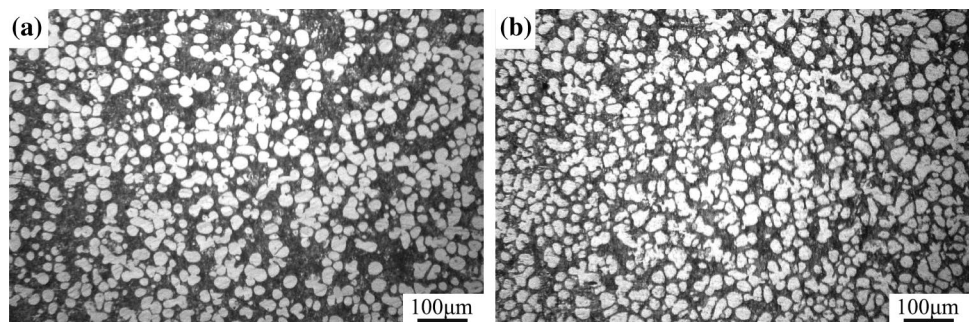


Fig. 4 The characteristic and preparation parameter of semi-solid slurry. **a** Characteristic parameter of semi-solid slurry and **b** preparation parameter of semi-solid slurry

Fig. 5 Microstructure of semi-solid slurry prepared by different water flow rate. **a** 0 L/h and **b** 1000 L/h



diameter and shape factor improving to 57 μm and reducing to 0.72, respectively. It could be got that through comparing Figs. 3c and 5a, b with the water flow rate increasing, the distribution of the primary $\alpha\text{-Al}$ grains in semi-solid slurry was gradually homogenized, but the spheroidization and refining of the primary $\alpha\text{-Al}$ grains improved firstly and then decreased. The reason of that might be related to the cooling rate caused by the water flow rate. When the water flow rate was 1000 L/h, the blocked slurry ratio was close to 25%. Therefore, the water flow rate of the water-cooled serpentine channel should be controlled at about 500 L/h.

3.3 Mechanical Properties of Tensile Samples

The semi-solid slurry with the same process parameters as sample “B” was used to produce the rheo-diecastings. As shown in Fig. 6a, the rheo-diecastings had more excellent mechanical properties than the traditional die castings in every mechanical property index. The average tensile strength, yield strength and elongation of the rheo-diecastings were about 325 MPa, 145 MPa and 4.5%, respectively, which improved by near 10%, 20% and 30%, respectively compared with the traditional die casting. It was noteworthy that the proportion of the serrated stress-strain curve caused by dynamic strain aging in stress-strain curve of rheo-diecastings was larger than that in traditional die castings, which might be related to the morphology, number and distribution of grains. Figure 6b was the vickers hardness curves of tensile samples, the test points were selected along the filling direction of the tensile samples, every three test points corresponded to the near-end region, middle region and far-end region, respectively. As shown in Fig. 6b, the vickers hardness of the tensile samples with same process parameter was close, the average hardness of the rheo-diecastings was about 125, which was higher about 20%–30% than that of the traditional die castings. The hardness of the

traditional die castings fluctuated in a great range compared with the rheo-diecastings through carefully observing. The reason of the fluctuation of the hardness might be similar to that of serrated stress-strain curve to some extent.

3.4 Macrostructure and Microstructure of Tensile Samples

The transversal macrostructure of the traditional die castings was divided into surface, transition region and center region from its surface to center by obvious defect bands [23, 24], as shown by arrows “A”, “B” and “C” in Fig. 7a. The microstructures of these regions were different, the grain size increased with the distance from the surface increasing. Without doubt, the liquid that firstly contacted the mold wall rapidly solidified into the fine equiaxed grain and formed the surface, as shown by region “A” in Fig. 7a, b. There were many small size dendrites and fracture dendritic arms in transition region, as shown in region “B” in Fig. 7a, b, which was related to the solidification of the surface, heating transfer speed decrease and the dendrite fracture. With the region away from the surface, the melt had great superheating and low heating transfer speed, resulting in the microstructure of the center region mainly consisting of the developed dendrites, as shown in Fig. 8a. Even the length of the principal axis was close to 1 mm, as shown in region “C” in Fig. 7a, c.

The transversal macrostructures and microstructure of the rheo-diecastings were quite different from those of the traditional die castings. The defect bands did not form in the rheo-diecastings, whose transversal macrostructures approximately consisted of surface and center region according to the morphology and size of the grain. Therefore, the microstructures of different regions were different. The residual liquid of the semi-solid firstly contacted mold wall and solidified into the fine equiaxed grain which was the main component forming the

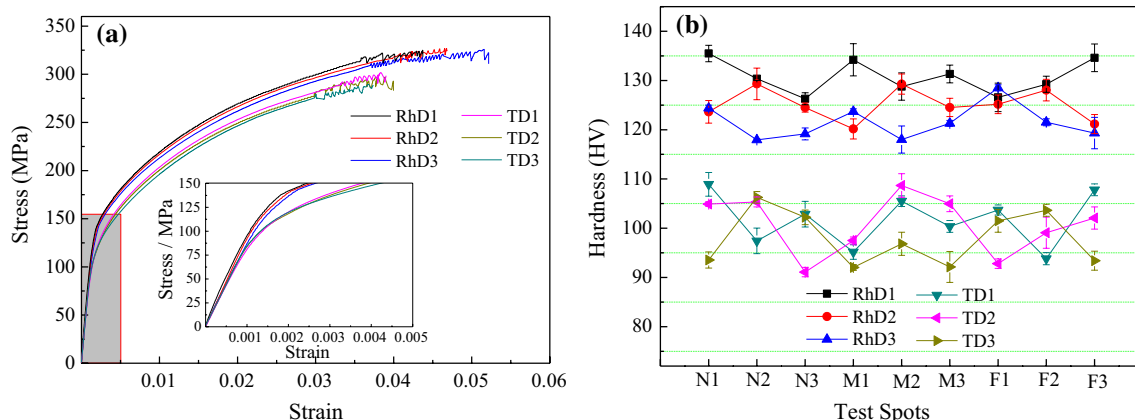


Fig. 6 The mechanical properties of the tensile samples. **a** Stress-strain curves of the tensile samples and **b** hardness curves of the tensile samples

Fig. 7 Macrostructure and microstructure of traditional die castings. **a** Macrostructure of traditional die castings; **b, c** microstructure of traditional die castings

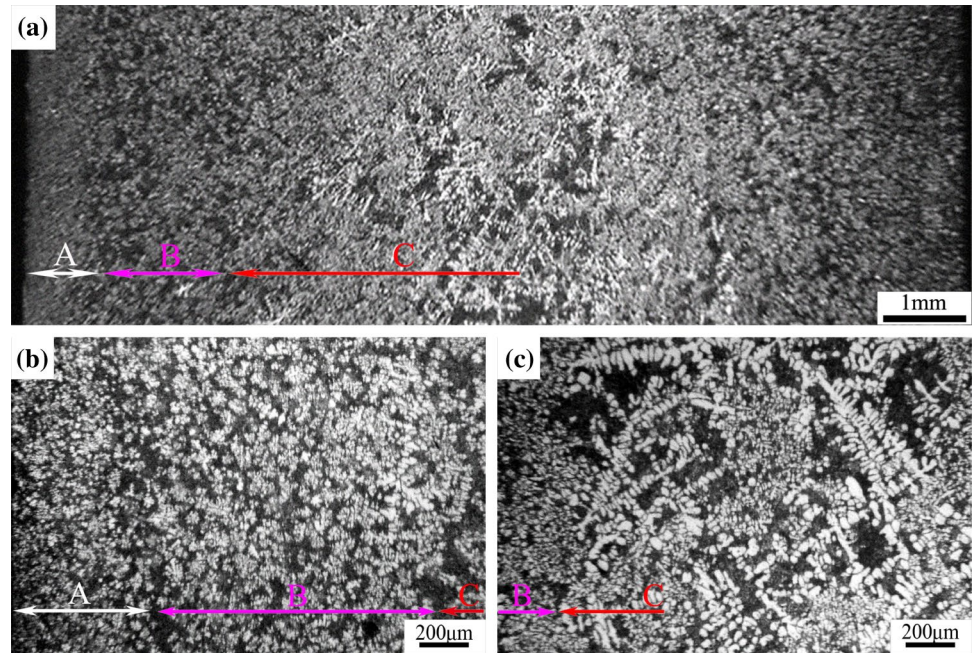
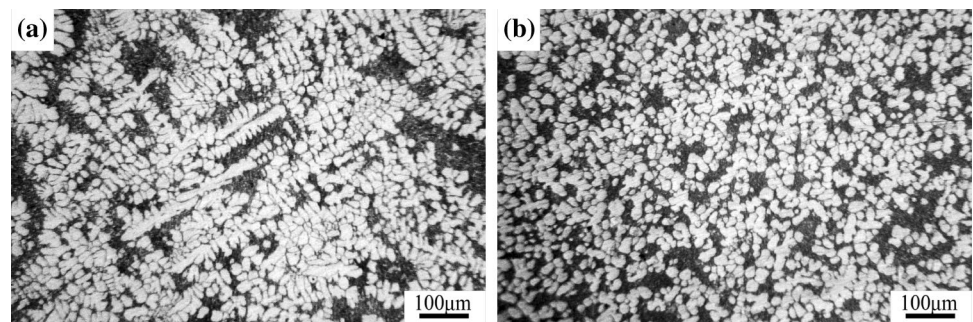


Fig. 8 Microstructure of traditional die castings and rheo-diecastings. **a** Microstructure of traditional die castings and **b** microstructure of rheo-diecastings



microstructure of the surface, in addition, there are a few near spherical grains in the surface, as shown by region "D" in Fig. 9a, b. In center region, mutual friction occurred among primary α -Al grains, therefore, the near-spherical or spherical primary α -Al grains and secondary α_2 -Al grains were composed of the microstructure of the center region [25, 26], as shown in region "E" in Fig. 9a, c. The grain diameter and shape factor of the primary α -Al grain were $32\ \mu\text{m}$ and 0.75, respectively, as shown in Fig. 8b. It is noteworthy that there seems to be a transition region between the surface and center region, where the morphology and the number of primary α -Al grains were slightly different from those of the above regions. It was mainly related to the viscosity of the semi-solid slurry, and heat transfer between the semi-solid slurry and the mold, as shown in Fig. 7a, b.

3.5 Fracture Morphology and Microstructure Nearby Fracture of Tensile Samples

Figure 10a was the macro fracture surface of the traditional die castings, which was mainly composed of a large area of macro solidification defects, as shown by red rectangle, quite a proportion of headstand "Y" pattern cracks with head pointing at macro defects, as shown by white arrows. It can be concluded that its fracture mode was mainly brittle fracture [27]. The micro fracture surface of the traditional die casting corresponding to the yellow rectangle in Fig. 10a presented the typical rocky pattern and radial river pattern that was short and curved. Moreover, the two patterns were separated by a clear boundary that indicated by red dotted line in Fig. 10b. The region "B" corresponding to rocky pattern had obvious solidification defects, which were most

Fig. 9 Macrostructure and microstructure of rheo-diecastings. **a** Macrostructure of rheo-diecastings; **b, c** microstructure of rheo-diecastings

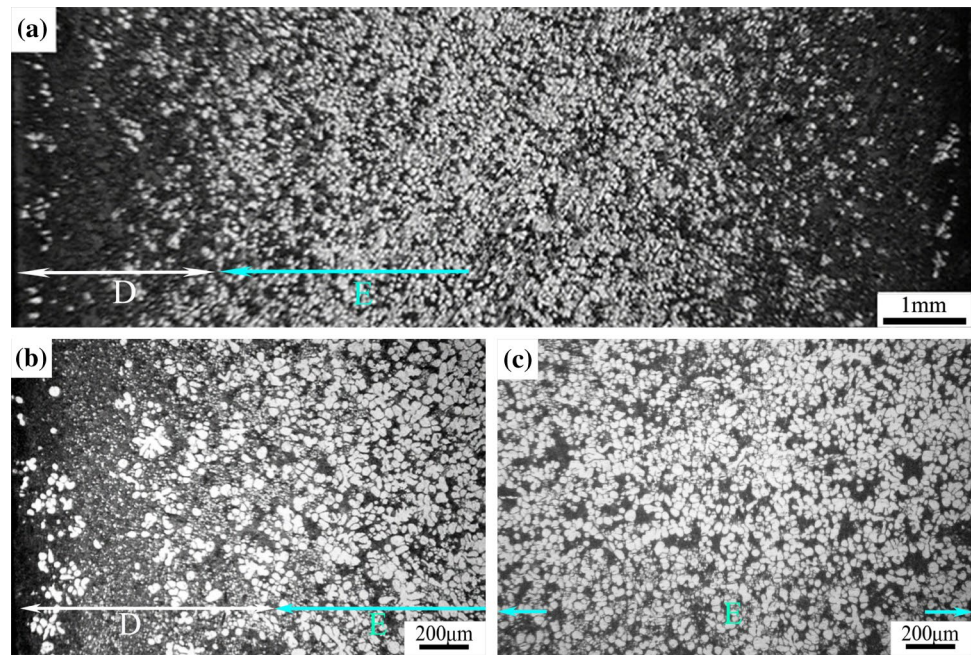
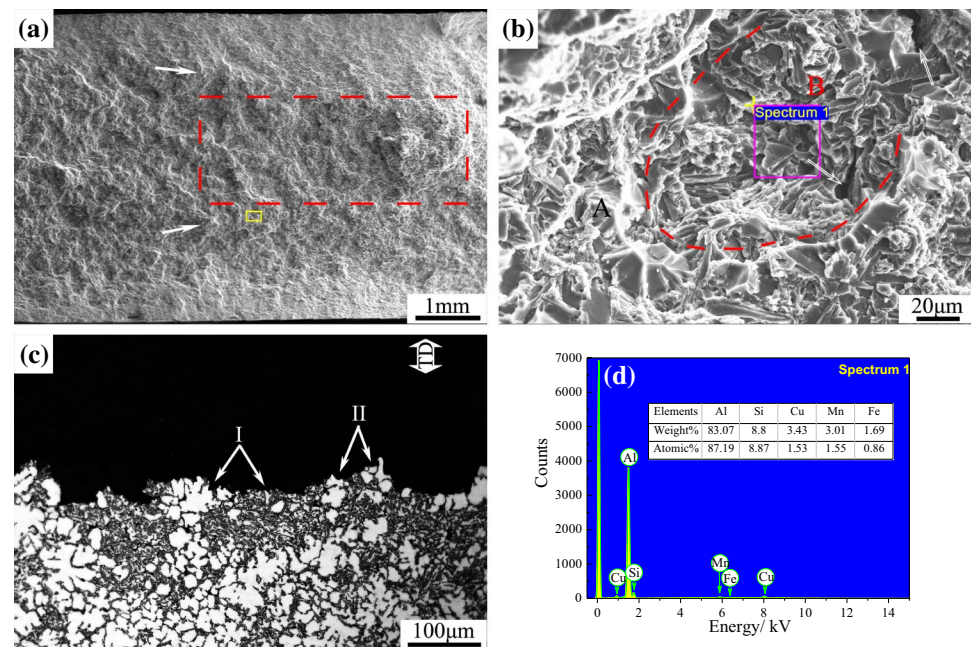


Fig. 10 Fracture morphology and microstructure nearby fracture of traditional die castings. **a** Macro fracture of traditional die castings; **b** micro fracture of traditional die castings; **c** EDS of brittle fracture and **d** microstructure nearby fracture of traditional die castings

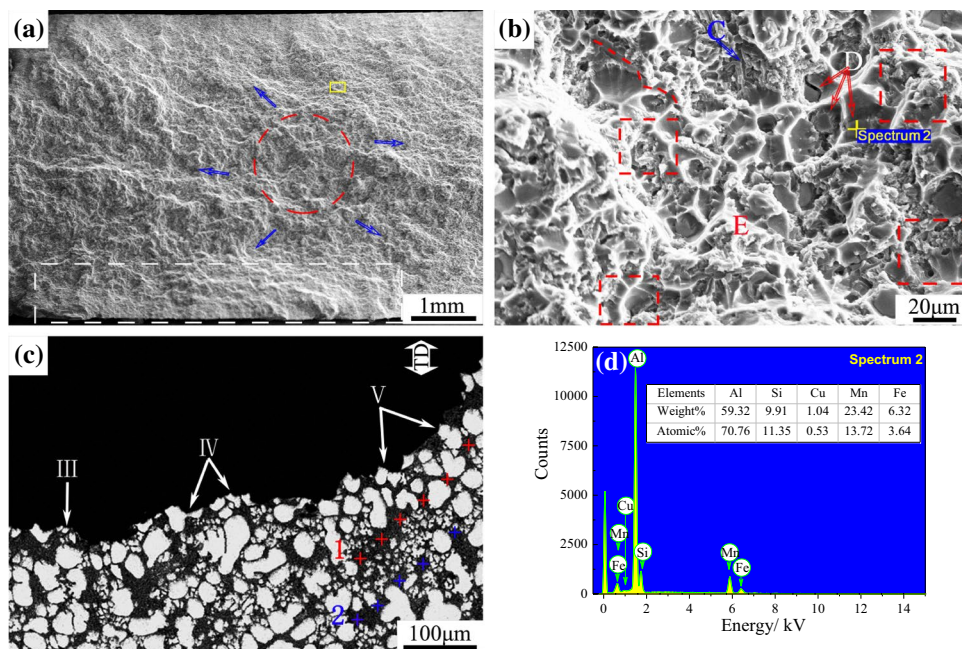


likely to be the crack origin, as shown in Fig. 10b. Therefore, the micro fracture mechanism of the region "B" was intergranular brittle fracture, as shown by "I" in Fig. 10c. Moreover, the Fig. 10d showed the microstructure nearby the fracture was most likely to be formed as the residual liquid solidified finally. The region "A" was composed of the radial river pattern, the secondary cracks, tear ridges and small quasi-cleavage facets, as shown in Fig. 10b, what's more, Fig. 10c showed the fracture surface was relatively flat and straight, which illustrated its micro fracture mechanism was

brittle quasi-cleavage. The cracks developed in the form of transgranular fracture, as shown by "II" in Fig. 10c.

When the rheo-diecasting replaced the traditional die casting, the fracture mode of the tensile samples changed from brittle fracture to ductile fracture. The fibrous region, radial region and shear lip could be easily identified in the macro fracture surface of the rheo-diecastings, as illustrated by red circle, blue arrows and white rectangle in Fig. 11a, respectively, which showed the characteristics of ductile fracture to a certain extent. The micro fracture surface of

Fig. 11 Fracture morphology and microstructure nearby fracture of rheo-diecastings. **a** Macro fracture of rheo-diecastings; **b** micro fracture of rheo-diecastings; **c** EDS of dimple fracture and **d** Micro-structure nearby fracture of rheo-diecastings



the position that corresponding to the yellow rectangle in Fig. 11a showed that the micro fracture mechanism of the rheo-diecastings contained the intergranular brittle fracture, the dimple fracture and quasi-cleavage fracture, as shown by "C", "D" and "E" in Fig. 11b. The proportion of intergranular brittle fracture was quite small, only a few grains like "III" remaining its integrity and without deformation, as shown in the Fig. 11c. Majority of proportion of the micro fracture morphology presented the dimple, secondary crack, tear ridge and small quasi-cleavage facet. Therefore, the micro fracture mechanism of the rheo-diecastings was mainly mixed-fracture mechanism of dimple and quasi-cleavage. The dimple fracture of the rheo-diecastings was mainly the form of intergranular. There were obvious second phase particles at the bottom of the dimples, and the brittle crack at the bottom of the dimple was the proof, as shown by red arrows "D" in Fig. 11b. This kind of the second phase particles were analyzed by energy dispersive X-ray spectroscopy, as shown in Fig. 11d, it was most likely to be Al–Si–Mn(Fe) compounds. Therefore, the second phase particles were likely to be the crack origin of the dimples fracture. The residual liquid had large quantities of the solute and inclusions, resulting in the interface adhesion between the secondary solidification microstructure and the primary α -Al grains being weak. Therefore, the primary α -Al grains with deformation basically remained their integrity, as shown by "V" in Fig. 11c. The quasi-cleavage fracture was mainly ductile transgranular fracture. There were many small dimples in the tear ridges and the primary α -Al grains deformed along the tensile direction, and they were shown by red dotted line in Fig. 11b and by "IV" in Fig. 11c, respectively. Most noteworthy, there were several obvious deformation bands

nearby the fracture, which had an angle of nearly 45° with the tensile direction and terminated at primary α -Al grains, as shown by "+" in Fig. 11c.

4 Discussion

When the water-cooled serpentine channel pouring process was used to prepare semi-solid slurry, the chilling effect of the water-cooled inner wall made a temperature boundary layer with large sub-cooling degree generate in the melt near the inner wall, which reduced the critical nucleation energy of melt. Moreover, the inner wall also acted as the heterogeneous nucleation substrate. As a result, there were a number of the α -Al nucleus forming on or nearby the inner wall. They were brought into melt by "self stirring" of melt forming the semi-solid slurry, which was collected by stainless steel crucible and quenched by water. In above process, the secondary α_2 -Al grains unavoidably formed on the crucible wall and were brought into melt by the "impact stirring" of the subsequent melt, meanwhile, the primary α -Al grains got a certain degree of Ostwald ripening [28].

Under the condition of the same water flow rate, the higher pouring temperature was bad for the preparation of semi-solid slurry. On the one hand, the higher the pouring temperature was, the smaller the sub-cooling degree of the melt was, and the lower the nucleation ratio of the melt was. The relationship between nucleation ratio and sub-cooling degree could be expressed by formula (1) [29]. On the other hand, the α -Al nucleus might be remelted by washing and stirring of the subsequent melt with high temperature, resulting in the effective nucleation ratio decreasing. Therefore,

the effective nucleation ratio increased with the decrease of pouring temperature. The high nucleation ratio of the melt could make the concentration field and temperature field around the primary α -Al grains overlap, which inhibited the preferred growth of primary α -Al grains and made primary α -Al grain grow in the spherical form. However, when the pouring temperature was too low, the high nucleation ratio of the melt made a part of the α -Al nucleus grow up and firmly attached on the inner wall instead of being brought into melt, resulting in the blocked slurry ratio increasing.

$$N_s = A_s \exp \left[-\frac{\Delta G_A}{kT} \right] \exp \left[-\frac{\alpha \sigma^3 T_m^2}{(L_m \Delta T)^2} \cdot \frac{2 - \cos \theta + 3 \cos^2 \theta}{4} \right] \quad (1)$$

where A_s is a constant, ΔG_A is the diffusion activation energy of atoms across the liquid/solid interface, k is the Boltzmann constant, T is thermodynamic temperature, α is the shape factor of nucleation (spherical nucleus: $\alpha = 16\pi/3$), σ is solid/liquid interface energy, L_m is the latent heat, ΔT is sub-cooling degree, and θ is wetting angle.

In addition, the cooling rate and sub-cooling degree of the melt were related to the water-cooling flow rate, and affected the nucleation ratio of the melt. The effect of the cooling rate on the nucleation ratio of the melt could be described by formula (2) [30].

The larger water-cooling flow rate made the melt have higher cooling rate, resulting in the nucleation ratio of the melt being higher. Moreover, the high cooling rate could restrain the diffusion of solute and hinder the growth of primary α -Al grain. However, the α -Al nucleus would easily and rapidly grow into dendrites under the too high cooling rate, which made the quality of the semi-solid slurry decrease. Therefore, the semi-solid slurry firstly optimized and then deteriorated, and the blocked slurry ratio increased with the water-cooling flow rate increasing.

$$N_c = 10^{c_o - m \cdot \lg \left[\frac{2 - 3 \cos \theta + \cos^2 \theta}{4} \right]} \cdot \frac{R_c}{S_v V} \quad (2)$$

where c_o is a constant, m is a regression coefficient related to materials ($m_{Al} = 0.54$), θ is wetting angle, R_c is cooling rate, S_v is surface area of the effective heterogeneous core, V is volume of melt.

Although the semi-solid slurry used in the rheo-diecasting was the same as that of the water quenched semi-solid slurry, their microstructures were quite different through comparing the Fig. 3c with Fig. 9c, which was related to their cooling type [31]. The semi-solid slurry was transferred into shot sleeve by a preheated preservation ladle within 3 seconds, which was bad for nucleation of the residual liquid. Moreover, it was difficult for the primary α -Al grains to grow and ripen. Therefore, it could be assumed that the semi-solid slurry in shot sleeve

approximately approached that just prepared. The injection pressure was the main reason that made the microstructure of the rheo-diecastings different from that of the water quenched semi-solid slurry. During rheo-diecasting, the injection pressure could accelerate interfacial heat transfer, improve melting point of the alloy and increase nucleation ratio. During the filling of the semi-solid slurry, it could be regarded as a high-speed droplet. The impact pressure of the droplet on the mold surface could be expressed as $P = c\rho v$. Where P is impact pressure, ρ is the density of the semi-solid slurry, v is the filling velocity, c is a time-dependent constant. Therefore, the injection pressure would greatly increase the heat transfer between the semi-solid slurry droplet and the mold [32]. The effect of the injection pressure on the melt point of the alloy was described by formula (3) [33], and the critical nucleation radius of the melt under the injection pressure was expressed by formula (4) [34]. Therefore, the residual liquid rapidly solidified into small size secondary α_2 -Al grains, as a result, the primary α -Al grains did not have solute to grow and had no time to ripen.

$$dT_p = \frac{T_m \Delta V}{L_m} dP \quad (3)$$

$$r_c = \frac{2\sigma_{ls} T_m}{L_m \Delta T + K\epsilon T_m P} \quad (4)$$

where dT_p is the variation of the melt point, T_m is the melt point at standard atmosphere pressure, ΔV and ΔT are the volume difference of solidification and the sub-cooling degree under injection pressure, respectively, L_m is the crystallize latent heat, r_c is the critical nucleation radius, σ_{ls} is the solid-liquid interfacial tension, K is the constant, ϵ is the shrinkage ratio, and P is the injection pressure.

Besides, the cooling rate of the semi-solid slurry was very great under fast mold filling, which could affect the grain diameter of the primary α -Al grains, the relation of the cooling rate and grain diameter could be expressed by an empirical formula (5) [35]. Therefore, both the grain diameter and shape factor of the primary α -Al grains were smaller.

$$D = BT_c^{-k} \quad (5)$$

where D is grain diameter, B and k are the constants related to materials [typically $20 < B < 160 \mu\text{m} (\text{K/s})^k$ and $0.25 < k < 0.5$], T_c is cooling rate.

The mechanical properties of the tensile samples was related to their microstructures that depended on their solidification mode. The surfaces of the traditional die castings and rheo-diecastings were similar, and they were composed of the fine equiaxed grains, as shown in Figs. 7a

and 9a. Under the injection pressure, a part of the residual liquid of the semi-solid slurry easily formed the leading liquid, which firstly contacted the mold wall and rapidly solidified into the fine equiaxed grains, whose solidification mode approximated to that of the liquid. Because the leading liquid fraction of the semi-solid slurry was low, the surface of the rheo-diecastings was narrower than that of the traditional die casting, and the segregation defect was effectively eliminated, as shown in Fig. 9a. What's more, there were a few primary α -Al grains in the surface of the rheo-diecasting. The differences of the surface of the tensile samples mentioned above were not enough to make their mechanical properties differ greatly. The mechanical properties of the tensile samples were mainly decided by microstructures of the center region that accounted for the half or more than half the proportion of the tensile samples. The center region of the traditional die castings was much narrower than that of the rheo-diecastings, and their microstructures were fundamentally different. During traditional die casting, the melt in center region away from the surface preferred to solidify into dendrites and rapidly grew up to developed dendrites along the direction of heat dissipation, as shown in Fig. 7c. As a result, the dendrites distributed unevenly, the number of the dendrites was small, and the shrinkage porosity and inclusions easily took place among the developed dendrites or dendritic arms. Therefore, the center region of the traditional die castings was most likely to be the place where the crack origin started in tensile test. During rheo-diecasting, with the leading liquid coming out from the residual liquid, the residual liquid reserved in center region reduced, and the viscosity of the semi-solid slurry increased. The residual liquid in center region rapidly solidified into the small size secondary α_2 -Al grains. The primary α -Al grains was retained in the center region because of the high viscosity of the semi-solid slurry. Therefore, the center region was composed of large number of primary α -Al grains and secondary α_2 -Al grains, as shown in Fig. 9c. The distribution, grain size and number of the grains in rheo-diecastings were more excellent than those in traditional die castings. It meant that there were more grains involved in deformation of the rheo-diecastings, which could be used to explain the reason why the rheo-diecastings had obvious dynamic strain aging, steady hardness, high the tensile strength and yield strength.

5 Conclusions

- 1 Under the condition of the same water-cooling flow rate, the average grain diameter and shape factor of the primary α -Al grains decreased and increased, respectively with the pouring temperature decreasing. Besides, when

the pouring temperature was the same, there was an optimum water-cooling flow rate for preparing the excellent semi-solid slurry. The optimum matching parameters of pouring temperature and water-cooling flow rate were 630 °C and 500L/h, respectively.

- 2 The mechanical properties of the tensile samples were related to their solidification mode. The semi-solid slurry could effectively reduce the solidification defects and improve the microstructure of the rheo-diecastings. A large number of the small size primary α -Al grains with uniform distribution were involved in the deformation of the rheo-diecastings, resulting in the mechanical properties of the rheo-diecastings being more excellent than those of the traditional die castings.

Acknowledgements National Basic Research Program of China (2011CB606300) supported this work.

References

1. Z. Fan, Semisolid metal processing. *Int. Mater. Rev.* **47**(2), 49–85 (2002)
2. M.C. Flemings, Behavior of metal alloys in the semisolid state. *Metall. Trans. B* **22**(3), 269–293 (1991)
3. B.K. Kang, C.P. Hong, Y.S. Jang, B.H. Choi, L. Sohn, Effect of casting parameters on the microstructure and mechanical properties of ADC10 alloys using a semisolid die casting and heat treating process. *Mater. Trans.* **57**(3), 410–416 (2016)
4. M. Li, Y.D. Li, G.L. Bi, X.F. Huang, T.J. Chen, Y. Ma, Effects of melt treatment temperature and isothermal holding parameter on water-quenched microstructures of A356 aluminum alloy semi-solid slurry. *Trans. Nonferrous Met. Soc. China* **28**(3), 393–403 (2018)
5. H.X. Cao, M.Y. Hao, C. Shen, P. Liang, The influence of different vacuum degree on the porosity and mechanical properties of aluminum die casting. *Vacuum* **146**, 278–281 (2017)
6. S.Y. Li, D.J. Li, X.Q. Zeng, W.J. Ding, Microstructure and mechanical properties of Mg–6Gd3Y–0.5Zr alloy processed by high-vacuum die-casting. *Trans. Nonferrous Met. Soc. China* **24**(12), 3769–3776 (2014)
7. T. Ito, T. Takikita, I. Miki, Wheels and Other Automotive Parts Through the Pore-Free Die Casting Process: SAE International Congress and Exposition, Detroit, Michigan, USA, 1991, SAE Technical Paper Series-910552, pp. 1–12 (1991)
8. G. Bar-Meir, Analysis of mass transfer process in the pore free technique. *J. Eng. Mater. Technol.* **117**(2), 215–219 (1995)
9. C.K. Jin, C.G. Kang, Semi-solid forging process and die design in the production of aluminum thin plates. *Solid State Phenom.* **217–218**, 151–158 (2014)
10. D.K. Kirkwood, Semisolid metal processing. *Int. Mater. Rev.* **49**(5), 173–189 (1994)
11. R. Canyook, J. Wannasin, S. Wisuthmethangkul, M.C. Flemings, Characterization of the microstructure evolution of a semi-solid metal slurry during the early stages. *Acta Mater.* **60**(8), 3501–3510 (2012)
12. R.A. Martinez, M.C. Flemings, Evolution of particle morphology in semisolid processing. *Metall. Mater. Trans. A* **36**(8), 2205–2210 (2005)

13. X.R. Chen, Z.F. Zhang, J. Xu, Effects of annular electromagnetic stirring processing parameters on semi-solid slurry production. *Trans. Nonferrous Met. Soc. China* **20**(Supplement 3), s873–s877 (2010)
14. P. Wang, G.M. Lu, J.Z. Cui, Microstructure of nearby liquidus semi-continuous casting aluminum alloy A356. *Acta Metall. Sin.* **38**(4), 389–392 (2002)
15. Z.Y. Zhao, R.G. Guan, X. Wang, C.M. Liu, Microstructure formation mechanism during a novel semisolid rheo-rolling process of AZ91 magnesium alloy. *Acta Metall. Sin. Engl.* **26**(4), 447–454 (2013)
16. D. Doutre, G. Hay, P. Wales, J.-P. Gabathuler, A new process for semi-solid forming. *Can. Metall. Quart.* **43**(2), 265–272 (2004)
17. S.S. Wu, G. Zhong, P. An, L. Wan, H. Nakae, Microstructural characteristics of Al–20Si–2Cu–0.4 Mg–1Ni alloy formed by rheo-squeeze casting after ultrasonic vibration treatment. *Trans. Nonferrous Met. Soc. China* **22**(12), 2863–2870 (2012)
18. X.L. Zhang, T.J. Li, S.S. Xie, H.T. Teng, J.Z. Jin, Microstructure evolution of A356 alloy in a novel rheocasting approach. *J. Mater. Process. Technol.* **209**(4), 2092–2098 (2009)
19. S. Ji, Z. Fan, M.J. Bevis, Semi-solid processing of engineering alloys by a twin-screw rheomoulding process. *Mater. Sci. Eng. A* **299**(1–2), 210–217 (2001)
20. N. Hirata, Y.M. Zulaida, M. Itamura, K. Anzai, Microstructure of Al alloy semi-solid slurry made in metallic vessel using vibrating plate. *Solid State Phenom.* **192–193**, 386–391 (2012)
21. J. Wannasin, Applications of semi-solid slurry casting using the gas induced semi-solid technique. *Solid State Phenom.* **192–193**, 28–35 (2012)
22. Z.Y. Liu, W.M. Mao, W.P. Wang, Z.K. Zheng, Preparation of semi-solid A380 aluminum alloy slurry by serpentine channel. *Trans. Nonferrous Met. Soc. China* **25**(5), 1419–1426 (2015)
23. A.K. Dahle, S. Sannes, D.H. St. John, H. Westengen, Formation of defect bands in high pressure die cast magnesium alloys. *J. Light Met.* **1**(2), 99–103 (2001)
24. C.M. Gourlay, H.I. Laukli, Dahle defect band characteristics in Mg–Al and Al–Si high-pressure die castings. *Metall. Mater. Trans. A* **38**(8), 1833–1844 (2007)
25. M. Hitchcock, Y. Wang, Z. Fan, Secondary solidification behaviour of the Al–Si–Mg alloy prepared by the rheo-diecasting process. *Acta Mater.* **55**(5), 1589–1598 (2007)
26. M. Li, Y.D. Li, G.L. Bi, X.F. Huang, T.J. Chen, Y. Ma, Solidification behavior of 6061 wrought aluminum alloy during rheo-diecasting process with self-inoculation method. *Trans. Nonferrous Met. Soc. China* **28**(5), 879–889 (2018)
27. J.L. González-Velázquez, *Fractography and Failure Analysis Structural Integrity* (Springer, Cham, 2018), pp. 49–69
28. L. Ratke, P.W. Voorhees, *Growth and Coarsening-Ostwald Ripening in Material Processing* (Springer, New York, 2002), pp. 117–126. <https://doi.org/10.1007/978-3-662-04884-9>
29. D. Turnbull, Formation of Crystal Nuclei in Liquid Metals. *J. Appl. Phys.* **21**(10), 1022–1028 (1950)
30. Z.Y. Jian, F.E. Chang, Y. Wen, Determination of critical nucleation rate of undercooled metal melt. *Progr. Nat. Sci.* **10**(1), 68–73 (2000) (**in Chinese**).
31. L. Li, R.F. Zhou, Q.H. Cen, D.H. Lu, Y.H. Jiang, R. Zhou, Effect of cooling rate on the microstructure of semi-solid Al–25Si–2Fe alloy during electromagnetic stirring. *Trans. Indian Inst. Metal.* **66**(2), 163–169 (2013)
32. J.L. Ge, H.D. Zhao, Q.Y. Hu, J.M. Gao, Z.M. Wang, Characteristics and influencing factors of skin microstructure in high pressure die casting aluminum alloys. *Spec. Cast. Nonferrous Alloys* **35**(11), 1174–1177 (2015) (**in Chinese**)
33. P.X. Qi, An expression for nucleation rate of crystallization under pressure. *Acta Metall. Sin.* **6**(20), B359–B364 (1984) (**in Chinese**)
34. Z.Y. Liu, W.M. Mao, W.P. Wang, Z.K. Zheng, Investigation of rheo-diecasting mold filling of semi-solid A380 aluminum alloy slurry. *Int. J. Min. Met. Mater.* **24**(6), 691–700 (2017)
35. T. Egami, W.L. Johnson, *Elements of Rapid Solidification-Fundamentals and Applications* (Berlin, 1998), pp. 24–42